N-14 overtone nuclear magnetic resonance of rotating solids

Zhehong Gan, Ivan Hung, Yusuke Nishiyama, Jean-Paul Amoureux, Olivier Lafon, Hiroki Nagashima, Julien Trebosc, Bingwen Hu

^{14}N overtone nuclear magnetic resonance of rotating solids

Zhehong Gan,[*,a] Ivan Hung,[a] Yusuke Nishiyama,[b,c] Jean-Paul Amoureux,[d,e] Olivier Lafon,[d,f] Hiroki Nagashima,[d] Julien Trébosc,[d] Bingwen Hu,[g]

[a] *Center of Interdisciplinary Magnetic Resonance, National High Magnetic Field Laboratory, 1800 East Paul Dirac Drive, Tallahassee, FL 32310, USA*
[b] *JEOL RESONANCE Inc., 3-1-2 Musashino, Akishima, 196-8558 Tokyo, Japan*
[c] *RIKEN-JEOL Collaboration Center, Tsurumi, Yokohama, Kanagawa 230-0045, Japan*
[d] *Univ. Lille, CNRS UMR 8181, UCCS Unit of Catalysis and Chemistry of Solids, F-59000 Lille, France*
[e] *Bruker France, 34 rue de l'industrie, 67166 Wissembourg, France*
[f] *Institut Universitaire de France, 1, rue Descartes, 75231 Paris Cedex 05, France*
[g] *School of Physics and Materials Science & Shanghai Key Laboratory of Magnetic Resonance, East China Normal University, Shanghai 200062, China*

[*] Corresponding author. Fax +1 850 644 1366.
E-mail address: gan@magnet.fsu.edu (Z. Gan).

ABSTRACT

By irradiating and observing at twice the ^{14}N Larmor frequency, overtone (OT) NMR is capable of obtaining ^{14}N^{OT} spectra without first-order quadrupolar broadening. Direct excitation and detection of the usually "forbidden" double-quantum transition is mediated by the perturbation from the large quadrupole interaction to the spin states quantized by the Zeeman interaction. A recent work (L.A. O'Dell, C.I. Ratcliffe, *Chem. Phys. Lett*. 514, 168, **2011**) has shown that ^{14}N^{OT} NMR under magic-angle spinning (MAS) can yield high-resolution spectra with typical second-order quadrupolar line shapes allowing the measurement of ^{14}N chemical shift and quadrupolar coupling parameters. This article has also shown that under MAS the main ^{14}N^{OT} peak is shifted by twice the sample spinning frequency with respect to its static position. We present the theory of ^{14}N^{OT} NMR of static or rotating samples and the physical picture of the intriguing spinning-induced shift in the second case. We use perturbation theory for the case of static samples and Floquet theory for rotating samples. In both cases, the results can be described by a so-called overtone parameter that scales down the ^{14}N^{OT} radio-frequency (*rf*) excitation and signal detection. This overtone parameter shows that the components of the *rf* field, which are transverse and longitudinal with respect to the magnetic field, are both effective for ^{14}N^{OT} *rf* excitation and signal detection. In the case of magic-angle spinning at angular frequency ω_r, the superposition of the excitation and detection components in the overtone parameter makes either the $+2\omega_r$ or $-2\omega_r$ term the dominant ^{14}N^{OT} signal, depending on the sense of sample spinning with respect to the magnetic field. This leads to an apparent ^{14}N^{OT} signal shifted at twice the spinning frequency. Features of ^{14}N^{OT} NMR spectra for both static and rotating samples are illustrated with simulations. The spinning induced shift and its dependence on spinning direction are confirmed experimentally by reversing the spinning direction and the field of the 36 Tesla series-connected hybrid magnet at the US National High Magnetic Field Laboratory.

Keywords: ^{14}N, overtone NMR, double-quantum transition, magic-angle spinning, quadrupole spin, Floquet theory, second-order quadrupular shift, spinning induced shift, serious-connected hybrid magnet

1. Introduction

Nuclear magnetic resonance (NMR) is a powerful tool for characterizing structure and dynamics of polycrystalline and disordered solids. Much of its success relies on its capability to resolve the chemical environments of atomic sites through slight variations of their resonance frequency. Nuclear spin interactions, such as chemical shift and dipolar or quadrupolar couplings, are anisotropic in nature and thus their orientation dependence leads to line broadening for powder samples. The anisotropic broadening must be averaged or reduced to achieve high spectral resolution. In solutions, the averaging occurs naturally due to rapid isotropic molecular tumbling. In solids, magic-angle spinning (MAS) of the sample averages out rank $l = 2$ spin interactions like dipolar coupling and chemical shift anisotropy (CSA).[1,2] For nuclear spin values larger than 1/2, the quest for high spectral resolution is confronted by the much larger interaction between the electric field gradient (EFG) and the electric quadrupole moment of the nucleus. The magnitude of the quadrupole interaction is often in the megahertz range, far larger than the fastest sample spinning frequency available. Fortunately, the first-order quadrupole interaction vanishes for the $+1/2 \leftrightarrow -1/2$ central transition of half-integer spins, allowing for its spectral acquisition without the large first-order broadening. The remaining second-order interaction is much smaller and can be partially reduced with MAS. Innovative methods like double rotation (DOR),[3] dynamic angle spinning (DAS),[4,5] multiple-quantum and satellite transition MAS (MQMAS and STMAS),[6,7] have been developed for the complete removal of the second-order quadrupolar broadening that has angular dependence up to rank $l = 4$. High magnetic fields can also reduce directly the second-order broadening, making solid-state NMR of quadrupolar nuclei one of the most important driving forces for high-field NMR.[8-10] The capability to obtain high spectral resolution has indeed

facilitated the widespread use of solid-state NMR for quadrupolar nuclei, which constitute the majority of isotopes in the Periodic Table.[11,12]

^{14}N is the most abundant isotope (99.65%) of nitrogen, an important element for all branches of chemistry, and one of the few nuclei in the Periodic Table with an integer spin. It is a spin S = 1 nucleus with a moderate quadrupole moment (20.44×10^{-31} m^2).[13] The direct NMR detection of ^{14}N nuclei in solids is challenging as it often requires specialized experimental approaches in order to excite and observe spectra that are typically several MHz wide (e.g. broadband MAS, field- or frequency-stepped piecewise acquisition, broadband frequency sweep pulses, etc.).[14-38] Obtaining site resolution is even more difficult for solids containing distinct ^{14}N sites. For samples with ^{13}C or ^{1}H nuclei near nitrogen sites, two-dimensional (2D) MAS experiments, like heteronuclear multiple-quantum correlation (HMQC), have been introduced to observe ^{14}N nuclei indirectly, partially overcoming the resolution and sensitivity difficulties of direct observation.[39-54] In this work, we focus on an approach, called nitrogen-14 overtone (^{14}N^{OT}) NMR, which directly excites and acquires ^{14}N spectra at twice its Larmor frequency. The m = +1 ↔ −1 double-quantum (DQ) transition is usually considered as forbidden, but it can become directly observable in the presence of large quadrupole interactions. The main advantage of ^{14}N^{OT} NMR is that the first-order quadrupolar broadening vanishes similarly to the central transition of half-integer nuclei. ^{14}N^{OT} NMR was first demonstrated experimentally by LeGros and Bloom,[55,56] and later applied to biomolecules.[57-60] ^{14}N^{OT} spectra of rotating samples have been recorded by Tycko and Opella, aiming at further line narrowing of CSA and second-order quadrupolar broadenings. However, for the sample selected and the low magnetic field and spinning frequency used, the spectra were found to be complicated by overlapping spinning sidebands. As a result, no significant line narrowing was materialized by sample rotation at that time.[57] On the theoretical

aspect, $^{14}N^{OT}$ NMR is different from conventional NMR with single-quantum excitation and detection. Tycko and Opella developed a formalism based on perturbation theory.[57] Two later works by Marinelli et al.[61] and Trease et al.,[62] provided more general descriptions in the form of density operators. They also explored the possibilities of applying advanced methods like DOR and DAS to completely average the quadrupolar broadening of $^{14}N^{OT}$ spectra. Numerical simulations were performed, which indicated that possible complications may occur if those methods, which were developed originally for half-integer quadrupolar nuclei, were applied to $^{14}N^{OT}$. However, no experimental demonstration was performed.

Recently, O'Dell and Ratcliffe published an experimental study of $^{14}N^{OT}$ NMR under MAS using higher magnetic fields, faster spinning rates and samples with smaller quadrupolar couplings.[63] Simple $^{14}N^{OT}$ MAS spectra were obtained with line shapes typical of second-order quadrupolar patterns, showing potential for measuring ^{14}N chemical shifts and quadrupolar coupling parameters. One of their main findings is that the $^{14}N^{OT}$ peak position shifts under MAS by twice the spinning frequency (ω_r) with respect to the non-spinning case. A brute-force simulation has confirmed this shift and predicted that its sign depends on the relative sense of spinning with respect to the magnetic field.[64] However, no theory or explanation was given for this intriguing feature. Recently, overtone excitation and detection have also been combined with double rotation, and the results showed that DOR can completely cancel the second-order quadrupolar broadening of $^{14}N^{OT}$ spectra.[65] All these experimental observations have renewed our interest in reexamining the $^{14}N^{OT}$ NMR theory, particularly under sample rotation.

In this article, we analyze the results observed in one-dimensional pulse-and-acquire $^{14}N^{OT}$ experiment. First, the $^{14}N^{OT}$ NMR theory for the time independent case of static samples is presented, using a density operator formalism similar to the work of Marinelli et al.[61] and Trease

et al..[62] An overtone parameter, ξ, is introduced such that $^{14}N^{OT}$ NMR can be described in a similar way as NMR applied to spin $S = 1/2$ nuclei. In the case of rotating samples, Floquet theory is used to treat this time dependent problem to obtain analytical expressions for the excitation and detection of the $^{14}N^{OT}$ transition. With spinning samples, the overtone parameter becomes time dependent and consists of five components ξ_k (k = 0, ±1 and ±2) modulated at 0, $\pm\omega_r$ and $\pm 2\omega_r$, respectively. The relative amplitudes of these terms reveal that under MAS rotation the dominant component is either the $+2\omega_r$ or $-2\omega_r$ sideband, depending on the spinning direction relative to the magnetic field $\boldsymbol{B}_0$, making the main overtone peak shift with the spinning frequency. In addition to the explanation of the intriguing MAS overtone features, the theory can also be used for rapid numerical simulations of overtone excitation and spectral line shapes.

2. Theory for static samples

2.1. In the laboratory frame

Let us consider a spin $S = 1$ nucleus in the laboratory frame (L) where the magnetic field is along the z axis. The Hamiltonian including the Zeeman, quadrupole and *rf* interactions in this frame can be written as:[66]

$$H^L = H_S^L + H_{rf}^L \quad (1)$$

$$H_S^L = \omega_0 S_z + H_Q^L \quad (2)$$

$$H_{rf}^L = 2\omega_1 (S_z \cos\theta_C + S_x \sin\theta_C) \cos(\omega_{irr} t + \phi) \quad (3)$$

$$H_Q^L = \omega_Q \sum_{m=-2}^{2} (-1)^m A_{2,m}^{Q,L} T_{2,-m}^{Q} \quad (4)$$

where H^L, H_S^L, H_{rf}^L and H_Q^L denote the total, spin, *rf* and quadrupolar Hamiltonians in the laboratory frame, respectively, and S_x and S_z denote the S spin angular momentum with respect to

the *x* and *z* axes, respectively. Here $\omega_0 = -\gamma B_0$ and $\omega_Q = \frac{2\pi e^2 qQ}{4hS(2S-1)}$ are the Larmor and quadrupolar coupling frequencies, respectively, where *eQ* is the electric quadrupole moment of the *S* spin and *eq* is the principal component of the EFG at the position of the *S* nucleus. The linearly modulated *rf* field, produced by the excitation coil tilted in the *xz*-plane at an angle θ_C with respect to the magnetic field $\boldsymbol{B}_0$, is described by its irradiation frequency ω_{irr}, phase ϕ, and nutation frequency $2\omega_1 = 2\gamma B_1$, where B_1 is the peak amplitude of the *rf* field. Fig. 1 depicts a solenoid coil where the $\boldsymbol{B}_1$ field generated by the coil consists of longitudinal, $S_z\cos\theta_C$, and transverse, $S_x\sin\theta_C$, terms in the *xz*-plane. The longitudinal component is usually negligible in conventional NMR, but not for $^{14}N^{OT}$ NMR and needs to be retained. The quadrupole interaction is expressed in the irreducible representation, where the spatial tensor components, $A^{Q,L}_{2,m}$, can be obtained from those, $A^{Q,P}_{2,m'}$, in the principal axis system *P* of the EFG tensor,

$$A^{Q,L}_{2,m} = \sum_{m'=-2}^{2} A^{Q,P}_{2,m'} D^2_{m'm}(\alpha_{PL}, \beta_{PL}, \gamma_{PL}) \tag{5}$$

where (α_{PL}, β_{PL}, γ_{PL}) are the Euler angles defining the orientation of the *P* frame in the *L* frame. The $A^{Q,P}_{2,m'}$ components are given by

$$A^{Q,P}_{2,0} = \sqrt{6},\ A^{Q,P}_{2,\pm1} = 0,\ A^{Q,P}_{2,\pm2} = -\eta_Q/2 \tag{6}$$

where η_Q is the asymmetry parameter of the EFG tensor. The elements of the Wigner matrix have the following form

$$D^2_{m'm}(\alpha_{PL}, \beta_{PL}, \gamma_{PL}) = \exp(-im'\alpha_{PL})\, d^2_{m'm}(\beta_{PL}) \exp(-im\gamma_{PL}) \tag{7}$$

where $d^2_{m'm}(\beta_{PL})$ are the reduced Wigner matrix elements. It can be shown that the complex conjugate of $A^{Q,L}_{2,m}$ is equal to

$$\left(A^{Q,L}_{2,m}\right)^* = (-1)^m A^{Q,L}_{2,-m} \tag{8}$$

The spin irreducible spherical tensor operators for the quadrupolar coupling are given by

$$T^Q_{2,0} = \frac{1}{\sqrt{6}}[3S_z^2 - S(S+1)\mathbf{1}]$$

$$T^Q_{2,\pm1} = \mp\frac{1}{2}[S_\pm S_z + S_z S_\pm] \quad (9)$$

$$T^Q_{2,\pm2} = \frac{1}{2}S_\pm S_\pm$$

where **1** denotes the unity operator. These tensor operators satisfy the equation

$$T^{Q,\dagger}_{2,m} = (-1)^m T^Q_{2,-m} \quad (10)$$

where $T^{Q,\dagger}_{2,m}$ denotes the adjoint operator of $T^Q_{2,m}$.

In the *L* frame, the evolution of the density operator σ^L(t) from its initial state σ^L(0) is governed by the Liouville-von Neumann equation

$$\frac{d\sigma^L(t)}{dt} = -i[H^L, \sigma^L(t)] \quad (11)$$

The expectation value of any observable represented by an operator O^L in the *L* frame, such as the NMR signal *s*(*t*), is given by

$$s(t) = Tr[O^{L\dagger}\sigma^L(t)] \quad (12)$$

Using the same coil tilted at the angle θ_C for detection, the $^{14}N^{OT}$ signal also contains longitudinal and transverse components similar to the *rf* irradiation, and hence the detection operator O^L_{det} can be written in the laboratory frame as

$$O^L_{det} = S_z\cos\theta_C + S_x\sin\theta_C \quad (13)$$

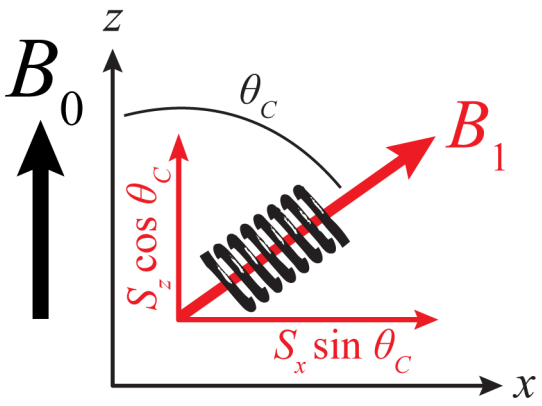

Fig.1. Depiction of the $\boldsymbol{B}_1$ *rf* field generated in the *xz*-plane by a *rf* solenoid coil at an angle θ_C with respect to the main magnetic field $\boldsymbol{B}_0$ as typically used in magic-angle spinning probes.

2.2. In the diagonal frame

2.2.1. Diagonal transformation of the spin Hamiltonian

We first transform the H_S^L Hamiltonian into the diagonal frame, *D*, where it is represented by a diagonal matrix, H_S^D, with elements that represent the energy levels of the *S* spin,

$$H_S^D = T^{-1} H_S^L T, \tag{14}$$

where *T* is a unitary matrix describing the transformation between the *D* and *L* frames, and $T^{-1} = T^{\dagger}$ is the inverse of the matrix *T*. In the absence of *rf* irradiation, the evolution operator or propagator, $\exp(-iH_S^D t)$, can be described simply by the energy levels. Similarly, the density and detection operators in the *D* frame can be expressed by the same transformation from those in the *L* frame as

$$\begin{aligned} \sigma^D(t) &= T^{-1}\sigma^L(t)T \\ O_{det}^D &= T^{-1}O_{det}^L T. \end{aligned} \tag{15}$$

Free evolution of the NMR signal can then be calculated in the *D* frame as:

$$\begin{aligned} s(t) &= \mathrm{Tr}\left[O_{det}^{D,\dagger} \exp(-iH_S^D t)\, \sigma^D(0) \exp(iH_S^D t)\right] \\ &= \mathrm{Tr}[T^{-1}O_{det}^{L,\dagger} T \cdot \exp(-iH_S^D t)\, T^{-1}\sigma^L(0) T \exp(iH_S^D t)] \end{aligned} \tag{16}$$

For $S = 1/2$ nuclei, this transformation is usually neglected because the perturbations from the chemical shifts, scalar and dipolar interactions to the spin states quantized by the Zeeman interaction are very small compared with the much larger Larmor frequency. Thus, the energy levels of the H_S^D matrix can then be obtained by simply discarding the small off-diagonal terms of all spin interactions that do not commute with the Zeeman Hamiltonian. Under this 'secular' approximation the NMR signal excitation and detection operators, usually a linear combination of S_x, S_y and S_z, have non-zero elements connecting only the single-quantum transitions. Therefore,

multiple-quantum or overtone transitions are 'forbidden', which means that they cannot be directly excited and detected. It must be mentioned that in the form of multi-dimensional experiments, multiple-quantum transitions can be easily detected indirectly via spin coherence transfer through single-quantum signal observation[42,44,49,53,67,68] including the overtone transition of ^{10}B with $S = 3$ reported recently.

The diagonal transformation T is the key point for $^{14}N^{OT}$ NMR, as it makes direct excitation and detection of the forbidden double-quantum (DQ) transition possible. Indeed, in the case of large quadrupole interactions, H_Q^L contains sizable off-diagonal non-secular elements that can be written for $S = 1$ nuclei (e.g., ^{14}N) as:

$$H_Q^L - \omega_Q A_{2,0}^{Q,L} T_{2,0}^Q = \omega_Q \begin{bmatrix} 0 & A_{2,-1}^{Q,L}/\sqrt{2} & A_{2,-2}^{Q,L} \\ -A_{2,1}^{Q,L}/\sqrt{2} & 0 & -A_{2,-1}^{Q,L}/\sqrt{2} \\ A_{2,2}^{Q,L} & A_{2,1}^{Q,L}/\sqrt{2} & 0 \end{bmatrix} \quad (17)$$

Assuming $\omega_Q < \omega_0$, the derivation of the transformation matrix T and the resulting energy levels of matrix H_S^D can be treated to first-order with static perturbation theory in operator form [71]:

$$T \approx \mathbf{1} + \varepsilon V \text{ with } V = \sum_{m=\pm1,\pm2} (-1)^m A_{2,m}^{Q,L} T_{2,-m}^Q / m \quad (18)$$

where

$$\varepsilon = \omega_Q / \omega_0 \quad (19)$$

is the ratio between the quadrupole and Zeeman interactions. Using $T^{-1} = T^\dagger$ and Eqs. 8, 10 and 18, it can be shown that

$$T^{-1} \approx \mathbf{1} - \varepsilon V \quad (20)$$

2.2.2. The internal spin Hamiltonian in the diagonal frame

Using perturbation theory under static conditions and Eqs. 14, 18 and 20, we can derive the internal spin Hamiltonian in the diagonal frame

$$H_S^D \approx (\mathbf{1} - \varepsilon V)H_S^L(\mathbf{1} + \varepsilon V) = H_S^L + \varepsilon[H_S^L, V] - \varepsilon^2 V H_S^L V \quad (21)$$

By neglecting the highest-order term $\varepsilon^2 V H_S^L V$ and substituting H_S^L by Eq. 2, the above expression can be written as

$$H_S^D \approx \omega_0 S_z + H_Q^L + \varepsilon[\omega_0 S_z, V] + \varepsilon\left[H_Q^L, V\right] \quad (22)$$

By substituting H_Q^L by Eq. 4 and *V* by Eq. 18, we obtain

$$H_S^D \approx \omega_0 S_z + \omega_Q A_{2,0}^{Q,L} T_{2,0}^Q + \frac{\omega_Q^2}{\omega_0} \sum_{m'=-2}^{2} \sum_{m=\pm 1,\pm 2} \frac{(-1)^m}{m} A_{2,m'}^{Q,L} A_{2,m}^{Q,L} \left[T_{2,m'}^Q, T_{2,m}^Q\right] \quad (23)$$

$$\approx \omega_0 S_z + H_Q^{D,(1)} + H_Q^{D,(2)} \quad (24)$$

The third term in Eq. 22 cancels the off-diagonal elements ($m \neq 0$) of the second term for the diagonalization H_Q^L because of the commutation relation $\left[S_z, T_{2,-m}^Q\right] = -mT_{2,-m}^Q$ [72]. $H_Q^{D,(n)}$, n = 1 and 2, denote the first- and second-order quadrupole Hamiltonians in the *D* frame, respectively. We can disregard the off-diagonal elements of the third term in Eq. 23 and keep only the diagonal elements for $H_Q^{D,(2)}$

$$H_Q^{D,(2)} = \frac{\omega_Q^2}{\omega_0} \sum_{m=1}^{2} A_{2,m}^{Q,L} A_{2,-m}^{Q,L} \left[T_{2,-m}^Q, T_{2,m}^Q\right]/m \quad (25)$$

which for an isolated spin S = 1 nucleus is equal to

$$H_Q^{D,(2)} = \frac{\omega_Q^2}{\omega_0}\left(-A_{2,1}^{Q,L} A_{2,-1}^{Q,L} + A_{2,2}^{Q,L} A_{2,-2}^{Q,L}\right) S_z = \omega_Q^{(2)} S_z \quad (26)$$

The first-order quadrupole interaction, $\omega_Q A_{2,0}^{Q,L} T_{2,0}^Q$, vanishes for the DQ transition between energy levels +1 ↔ −1, and hence the Hamiltonian in the absence of *rf* irradiation describing the energy levels and transition frequencies for $^{14}N^{OT}$ NMR is given by

$$H_S^{DQ} = 2(\omega_0 + \omega_Q^{(2)}) S_z^{DQ} = \omega_{DQ} S_z^{DQ} \quad (27)$$

where $\omega_Q^{(2)}$ is the second-order quadrupole frequency. Here we have used a single-transition spin S = 1/2 operator S_z^{DQ} to describe the +1 ↔ −1 transition.[66] The factor of 2 in Eq. 27 comes from the reduction from the spin S = 1 S_z operator to the S = 1/2 single-transition operator, which shows that overtone NMR resonates at twice the Larmor frequency, i.e., $\omega_{DQ} = 2(\omega_0 + \omega_Q^{(2)})$.

2.2.3. In the rotating frame

To simplify calculations, we can define a frame R rotating at the irradiation frequency $\omega_{irr}/2$ around the z axis of the D frame. The rotation matrix can be described in the spin S = 1/2 double-quantum transition operator $R = \exp\left(i\omega_{irr}tS_z^{DQ}\right)$ for the transformation from the D to the R frame. In this frame, the internal spin Hamiltonian becomes

$$H_S^R = \Omega_{DQ}S_z^{DQ} = (\omega_{DQ} - \omega_{irr})S_z^{DQ} \tag{28}$$

where Ω_{DQ} is the resonance frequency offset of the DQ transition.

2.2.4. The detection operator

By combining Eqs. 15, 18 and 20, the detection operator in the D frame can be written as

$$\begin{aligned} O_{det}^D &= (\mathbf{1} - \varepsilon V)O_{det}^L(\mathbf{1} + \varepsilon V) \\ &= O_{det}^L + \varepsilon[O_{det}^L, V] - \varepsilon^2 V O_{det}^L V \\ &\approx O_{det}^L + \varepsilon[O_{det}^L, V] \end{aligned} \tag{29}$$

by neglecting the second-order term $\varepsilon^2 V O_{det}^L V$. As stated previously (Eq.13), the detection operator in the laboratory frame, $O_{det}^L = S_z\cos\theta_C + S_x\sin\theta_C$, has no element connecting the DQ transition. However, the diagonal transformation leads to non-vanishing DQ elements in the O_{det}^D operator. When deriving the commutator,

$$\varepsilon[O_{det}^{L}, V] = \varepsilon\left[S_z \cos\theta_C + S_x \sin\theta_C \, , \sum_{m=\pm1,\pm2}(-1)^m A_{2,m}^{Q,L} T_{2,-m}^{Q}/m\right] \qquad (30)$$

we only keep the double-quantum elements $T_{2,\pm2}^{Q}$ that give rise to a NMR signal oscillating at twice the Larmor frequency. All other elements are irrelevant for $^{14}N^{OT}$ NMR and hence can be discarded, which leads to

$$O_{det}^{D} \approx \varepsilon[\left(A_{2,-1}^{Q,L}\sin\theta_C - A_{2,-2}^{Q,L}\cos\theta_C\right)T_{2,2}^{Q} - \left(A_{2,1}^{Q,L}\sin\theta_C + A_{2,2}^{Q,L}\cos\theta_C\right)T_{2,-2}^{Q}] \qquad (31)$$

Again for simplicity, we use the single-transition operators to describe the DQ transition of $^{14}N^{OT}$ with the detection operator for the quadrature-detected $^{14}N^{OT}$ signal given by

$$O_{det}^{D} = -\varepsilon\left(A_{2,1}^{Q,L}\sin\theta_C + A_{2,2}^{Q,L}\cos\theta_C\right)S_{-}^{DQ} = \xi^* S_{-}^{DQ} \qquad (32)$$

where the overtone parameter ξ is defined as

$$\xi = \varepsilon\left(A_{2,-1}^{Q,L}\sin\theta_C - A_{2,-2}^{Q,L}\cos\theta_C\right) \qquad (33)$$

2.2.5. The *rf* Hamiltonian

Let us now consider the case of overtone excitation with *rf* irradiation near twice the Larmor frequency. We assume the *rf* Hamiltonian to be small with respect to H_S^L, and hence it transforms into the *D* frame as

$$H_{rf}^{D} = T^{-1} H_{rf}^{L} T \qquad (34)$$

We can follow the same procedure used for the previous derivation of Eq. 31 and keep only the DQ elements for overtone excitation:

$$H_{rf}^{D} = 2\omega_1 \cos(\omega_{irr} t + \phi)\left(\xi T_{2,2}^{Q} + \xi^* T_{2,-2}^{Q}\right) \qquad (35)$$

The rapid oscillation of the *rf* Hamiltonian in the laboratory frame can be reduced by using the rotating frame *R* previously defined in Section 2.2.3:

$$H_{rf}^{R} = R^{-1}H_{rf}^{D}R$$

$$= \omega_1[(1+\exp[-i(2\omega_{irr}t+\phi)])\xi T_{2,2}^{Q}$$

$$+(1+\exp[i(2\omega_{irr}t+\phi)])\xi^{*}T_{2,-2}^{Q}] \quad (36)$$

Indeed, when we neglect the effects of the non-resonant rotating component of the *rf* field, this Hamiltonian becomes time-independent and can be written as

$$H_{rf}^{R} \approx \omega_1\left(\xi e^{-i\phi}S_{+}^{DQ} + \xi^{*}e^{i\phi}S_{-}^{\boldsymbol{DQ}}\right)$$

$$= 2\omega_1|\xi|\exp\left(-i\phi_{DQ}S_z^{DQ}\right)S_x^{DQ}\exp\left(i\phi_{DQ}S_z^{DQ}\right) \quad (37)$$

where

$$\phi_{DQ} = \phi + \arg(\xi^{*}) \quad (38)$$

Eqs. 28, 32 and 37 summarize the results of the $^{14}N^{OT}$ theory under static conditions. $^{14}N^{OT}$ NMR can be treated as conventional NMR of a fictitious spin $S = 1/2$ nucleus with a single DQ overtone transition between two energy levels. Both the *rf* excitation and detection is scaled by the overtone parameter in Eq. 33.

In the R frame, the equilibrium state is defined by the density operator $\sigma^{R}(0) \propto 2S_z^{DQ}$ when considering only the zeroth-order term in Eq. 15. The time evolution after pulse excitation is given by

$$\sigma^{R}(t > \tau_p) = \exp\left[-iH_S^{R}(t-\tau_p)\right]\exp\left(-iH_{rf}^{R}\tau_p\right)\sigma^{R}(0)$$

$$\times \exp\left(iH_{rf}^{R}\tau_p\right)\exp\left[iH_S^{R}(t-\tau_p)\right] \quad (39)$$

where τ_p is the pulse length and t denotes the time elapsed from the start of the pulse. S_x^{DQ}, S_y^{DQ} and S_z^{DQ} are three cyclically commutating spin $S = 1/2$ operators for the double-quantum transition. Using Eqs. 28 and 37, we obtain

$$\sigma^{R}(t > \tau_p) = 2\cos\left(2|\xi|\omega_1\tau_p\right)S_z^{DQ} - 2\sin\left(2|\xi|\omega_1\tau_p\right)$$

$$\times \left(\sin\left[\Omega_{DQ}\left(t-\tau_p\right)-\phi_{DQ}\right]S_x^{DQ}-\cos\left[\Omega_{DQ}\left(t-\tau_p\right)-\phi_{DQ}\right]S_y^{DQ}\right) \qquad (40)$$

Assuming that off-resonance effects can be neglected, i.e., the H_{rf}^R Hamiltonian is large with respect to H_S^R, the $^{14}N^{OT}$ signal can be calculated in the *R* frame as:

$$s\left(t>\tau_p\right) \propto \mathrm{Tr}\left[O_{det}^{R,\dagger}\sigma^R\left(t>\tau_p\right)\right]$$

$$= |\xi|\sin\left(2|\xi|\omega_1\tau_p\right)\exp\left(i\left[\omega_{DQ}\left(t-\tau_p\right)+\omega_{irr}\tau_p-\phi-\pi/2\right]\right) \qquad (41)$$

The overtone signal detection (Eq. 34) and *rf* excitation (Eq. 37) are scaled down by the same overtone parameter, $|\xi|$, which is proportional to the ratio between the quadrupolar coupling constant and the Larmor frequency: $\varepsilon = \omega_Q/\omega_0$. The overtone parameter is anisotropic through the single- and double-quantum elements of the quadrupole Hamiltonian, $A_{2,-1}^{Q,L}$ and $A_{2,-2}^{Q,L}$, respectively (Eq. 33), and therefore it depends on the molecular/crystallite orientation (Eq. 5). ξ is also sensitive to the *rf* coil orientation with respect to the magnetic field $\boldsymbol{B}_0$ as defined by the angle θ_C in Eq. 33. These features are unique to $^{14}N^{OT}$ NMR in which the overtone parameter plays a central role.

3. Theory for rotating samples

3.1. Periodically time-dependent spin Hamiltonian

We now consider a solid rotating in the *L* frame. The internal spin Hamiltonian, H_S^L, becomes time modulated, including the off-diagonal elements of the quadrupolar interaction that make the overtone transition detectable,

$$H_Q^L(t) = \omega_Q \begin{bmatrix} A_{2,0}^{Q,L}(t)/\sqrt{6} & A_{2,-1}^{Q,L}(t)/\sqrt{2} & A_{2,-2}^{Q,L}(t) \\ -A_{2,1}^{Q,L}(t)/\sqrt{2} & -A_{2,0}^{Q,L}(t)\sqrt{2/3} & -A_{2,-1}^{Q,L}(t)/\sqrt{2} \\ A_{2,2}^{Q,L}(t) & A_{2,1}^{Q,L}(t)/\sqrt{2} & A_{2,0}^{Q,L}(t)/\sqrt{6} \end{bmatrix} \quad (42)$$

The spatial tensor components, $A_{2,m}^{Q,L}$(t), can be obtained from those, $A_{2,m'}^{Q,P}$, in the *P* frame of the EFG tensor by two consecutive rotations, one from the laboratory to the rotor frame with the Euler angles ($-\omega_r t$, θ_C, 0) and the second from the rotor to the PAS frame (α_{PR}, β_{PR}, γ_{PR}):

$$A_{2,m}^{Q,L}(t) = \sum_{k,m'=-2}^{2} A_{2,m'}^{Q,P} D_{m'k}^{2}(\alpha_{PR}, \beta_{PR}, \gamma_{PR}) D_{km}^{2}(-\omega_r t, \theta_C, 0) \quad (43)$$

where

$$D_{m'k}^{2}(\alpha_{PR}, \beta_{PR}, \gamma_{PR}) = \exp(-i\alpha_{PR})\, d_{m'k}^{2}(\beta_{PR}) \exp(-ik\gamma_{PR}) \quad (44)$$

$$D_{km}^{2}(-\omega_r t, \theta_C, 0) = \exp(ik\omega_r t)\, d_{km}^{2}(\theta_C) \quad (45)$$

We assume here that the spinning axis and *rf* coil axis coincide at angle θ_C with respect to the $\boldsymbol{B_0}$ field, as it is usually the case in MAS probes. For rotating solids, The $A_{2,m}^{Q,L}$ components can thus be expanded as a Fourier series with respect to the angular rotation frequency ω_r,

$$A_{2,m}^{Q,L}(t) = \sum_{k=-2}^{2} a_m^k \exp(ik\omega_r t) \quad (46)$$

with

$$a_m^k = \sum_{m'=-2}^{2} A_{2,m'}^{Q,P} D_{m'k}^{2}(\alpha_{PR}, \beta_{PR}, \gamma_{PR}) d_{km}^{2}(\theta_C). \quad (47)$$

The quadrupolar Hamiltonian can thus be written as a sum of five matrices h_Q^k,

$$H_Q^L(t) = \omega_Q \sum_{k=-2}^{2} h_Q^k \exp(ik\omega_r t) \quad (48)$$

with

$$h_Q^k = \begin{bmatrix} a_0^k/\sqrt{6} & a_{-1}^k/\sqrt{2} & a_{-2}^k \\ -a_1^k/\sqrt{2} & -a_0^k\sqrt{2/3} & -a_{-1}^k/\sqrt{2} \\ a_2^k & a_1^k/\sqrt{2} & a_0^k/\sqrt{6} \end{bmatrix} \quad (49)$$

Here we assume that $\omega_r < \omega_Q$, and hence we must consider the terms with $k \neq 0$ in Eq. 48. Similar to the static case, we can focus only on the off-diagonal quadrupolar elements of Eq. 49 that make $^{14}N^{OT}$ NMR possible.

3.2. Floquet's theory and the diagonal tilted transformation

Floquet's theory is invoked to treat the periodic, modulated perturbations.[73,74] Floquet's theorem states that the propagator of a periodic Hamiltonian, $H(t)$, can be expressed in terms of a time dependent periodic operator, $T(t)$, and a constant diagonal Hamiltonian, H_S^D,

$$U(t) = T(t)\exp(-iH_S^D t)\,T(0)^{-1} \tag{50}$$

Assuming $\varepsilon = \omega_Q/\omega_0 < 1$ and $\omega_r \ll \omega_Q$, the $T(t)$ operator that diagonalizes the Hamiltonian can be obtained using a first-order perturbation treatment of the Floquet Hamiltonian [73,74].

$$T(t) = \mathbf{1} + \varepsilon \sum_{k=\pm1,\pm2} V_k \exp(ik\omega_r t) \tag{51}$$

where

$$V_k = \begin{bmatrix} 0 & a_{-1}^k/\sqrt{2} & a_{-2}^k/2 \\ -a_1^k/\sqrt{2} & 0 & -a_{-1}^k/\sqrt{2} \\ a_2^k/2 & a_1^k/\sqrt{2} & 0 \end{bmatrix} \tag{52}$$

3.3. The internal spin Hamiltonian

The H_S^D in Eq. 50 of the Floquet theory is related to the average Hamiltonian $\langle H \rangle$

$$\langle H \rangle = T(0) H_S^D T(0)^{-1} \tag{53}$$

Thus it can be calculated as in the static case (Eqs. 21 to 27), retaining only the diagonal and time-independent terms

$$H_S^D = 2(\omega_0 + \bar{\omega}_Q^{(2)}) S_z^{DQ} = \bar{\omega}_{DQ} S_z^{DQ} \tag{54}$$

Here, $\bar{\omega}_{DQ}$ is the time-averaged resonance frequency of the DQ transition. The time-averaged second-order quadrupole frequency (see Eq. 26) is given by

$$\bar{\omega}_Q^{(2)} = \frac{\omega_Q^2}{\omega_0} \sum_{k=-2}^{2} \left(-a_1^{-k} a_{-1}^{k} + a_2^{-k} a_{-2}^{k}\right) \tag{55}$$

This frequency can also be expressed as a function of second- and fourth-rank spatial tensors [74].

The diagonal tilted transformation can also induce a geometric phase term or so-called Berry's phase from the time dependent Hamiltonian to the averaged peak position for rotating samples. Berry's phase can be visualized as the solid angle encompassed by the sweeping quantization axis of the cyclic Hamiltonian.[75] The accumulation of Berry's phase can result in a shift proportional to the spinning speed and sensitive to the spinning direction with respect to the quantization axis as it was experimentally demonstrated by Nuclear Quadrupole Resonance (NQR) of a rotating single crystal at and near zero-field.[76] In the case of ^{14}N overtone at high fields, the quatization axis is just slightly off from the main magnetic field. The encompassed solid angle or the Berry's is small, in the order of $(\omega_Q/\omega_0)^2/4\pi$. Therefore the resulting shift can be estimated in the order of $(\omega_Q/\omega_0)^2\omega_r/4\pi$, ω_r/ω_Q smaller the second-order quadrupolar shift in Eq. (55). The Berry's phase may become observable at high fields under fast spinning.

3.4. The detection operator

The detection operator in the *D* frame, which is transformed into the *L* frame by the matrix *T*(*t*), is given by

$$O_{det}^{D} = T(t)^{-1} O_{det}^{L} T(t) \tag{56}$$

Following the same procedure we have used to derive Eq. 32 in the static case, we obtain for the overtone detection operator under sample rotation,

$$O_{det}^{D} = \xi_{rot}^{*}(t)\, S_{-}^{DQ} \tag{57}$$

where

$$\xi^*_{rot}(t,\theta_C) = \sum_{k=-2}^{2} \xi^*_k(\theta_C)\exp(ik\omega_r t) \quad (58)$$

$$\xi_k(\theta_C) = \varepsilon(a^k_{-1}\sin\theta_C - a^k_{-2}\cos\theta_C) \quad (59)$$

By inserting Eq. 47 into Eq. 59, we obtain

$$\xi_k(\theta_C) = \varepsilon\chi_k(\theta_C)\sum_{m=-2}^{2} A^{Q,P}_{2,m} D^2_{m,k}(\alpha_{PR},\beta_{PR},\gamma_{PR}) \quad (60)$$

with

$$\chi_k(\theta_C) = d^2_{k,-1}(\theta_C)\sin\theta_C - d^2_{k,-2}(\theta_C)\cos\theta_C \quad (61)$$

which provides the following expressions

$$\chi_0(\theta_C) = -\frac{3}{2}\sqrt{\frac{3}{2}}\cos\theta_C\sin^2\theta_C$$

$$\chi_1(\theta_C) = -\chi_{-1}(\pi-\theta_C) = 2\cos^2(\theta_C/2)(1+3\cos\theta_C)\sin^3(\theta_C/2) \quad (62)$$

$$\chi_2(\theta_C) = -\chi_{-2}(\pi-\theta_C) = -(2+3\cos\theta_C)\sin^4(\theta_C/2)$$

Equations (58), (60) and (61) show that for rotating samples the overtone parameter have five modulating components. The relative amplitudes among the five components are constants for all orientation in powder samples which are determined only by the angle of spinning and coil axis with respect to the magnetic field. In the next section, the numerical values of the constant show that either $k = 2$ or -2 component is dominant under magic-angle spinning leading to apparent overtone peak shifting at twice of the spinning frequency. This is the key finding from theory which explains the intriguing feature of ^{14}N overtone NMR observed experimentally under MAS.[63] Previous theoretic studies[57,61,62] have not gone far enough to reach this conclusion.

3.5. The *rf* Hamiltonian

The *rf* spin Hamiltonian can also be expressed in the *D* frame as

$$H_{rf}^{D} = T(t)^{-1} H_{rf}^{L} T(t) \tag{63}$$

Using the same procedure as in the static case, we can express the *rf* Hamiltonian in a frame *R* rotating at the irradiation frequency $\omega_{irr}/2$ around the *z*-axis of the *D* frame (section 2.2.3). Neglecting the non-resonant rotating component of the *rf* field, the *rf* spin Hamiltonian in such a *R* frame can be written into a form similar to Eq. 37 derived in the static case as

$$H_{rf}^{R} \approx \omega_1 \left(\xi_{rot}(t, \theta_C) e^{-i\phi} S_{+}^{DQ} + \xi_{rot}^{*}(t, \theta_C) e^{i\phi} S_{-}^{DQ} \right) \tag{64}$$

The sample spinning adds additional modulations to the oscillating *rf* field through the overtone parameter. With short *rf* pulses in the linear excitation regime, the contributions from the five modulating components are additive. We can express the overtone signal as

$$\begin{aligned} s\left(t > \tau_p\right) \propto & \sum_{k=-2}^{2} |\xi_k(\theta_C)| \sin\left(2|\xi_k(\theta_C)|\omega_1 \tau_p\right) \\ & \times \exp\left(i\left[\left(\bar{\omega}_{DQ} + k\omega_r\right)\left(t - \tau_p\right) + (\omega_{irr} + k\omega_r)\tau_p - \phi - \pi/2\right]\right) \end{aligned} \tag{65}$$

The overtone signal of rotating solids hence contains five modulating components, which lead to five resonances separated by the spinning frequency. Their appearance is similar to the spinning sidebands often seen in solid state NMR of rotating samples, however with a fundamental difference. Conventional spinning sideband intensities depend on the ratio between the magnitude of the observed NMR frequency modulation and the spinning frequency, and hence they diminish with faster spinning. On the contrary, the five overtone peaks do not result from the modulation of the ^{14}N second-order quadrupole interaction, which affects the resonance frequency of the overtone signal (Eq. 54), but from the modulation of the total quadrupole interaction, which affects the efficiency of excitation and detection of the overtone transition under sample rotation. The intensities of the five components are hence independent of the spinning frequency. Moreover, Eq. 62 shows that the relative intensity of the five overtone sidebands depends on the angle of the rotor axis, θ_C, which will be discussed later. When the CSA or the ^{14}N second-order quadrupole

interaction is larger than ω_r, the modulation of the overtone DQ frequency leads to extra spinning sidebands in addition to the five overtone components. These sidebands behave like conventional ones and thus disappear with higher spinning frequencies like those typically used experimentally in $^{14}N^{OT}$ NMR.

4. Results and discussions

The $^{14}N^{OT}$ NMR theory presented above centers on the overtone parameter, ξ or ξ_k for static or rotating conditions, respectively, which depends on the quadrupole interaction, the crystallite orientation, and the spinning/*rf* coil axis angle, θ_C, with respect to $\boldsymbol{B}_0$.

First, ξ and ξ_k scale both *rf* excitation and signal detection, and are proportional to the ratio between the quadrupole and Zeeman interactions through the parameter $\varepsilon = \omega_Q/\omega_0$ (Eqs. 33 and 59). Because of the scaling factor, $^{14}N^{OT}$ NMR may look a priori less favorable at high magnetic fields. However, there are several advantages with increasing B_0 magnetic field: (i) increase in spin polarization due to the Boltzmann factor, (ii) decrease of second-order quadrupolar line broadening, (iii) increase sensitivity due to the inductively detected NMR signal being proportional to frequency, (iv) increase in separation between various resonances through chemical shift differences. The overall overtone sensivity still increases with the magnetic field considering all these factors.[77]

Second, ξ and ξ_k depend on the molecular orientation through the $A_{2,-1}^{Q,L}$ and $A_{2,-2}^{Q,L}$ (see Eq. 33) or a_{-1}^{k} and a_{-2}^{k} (see Eq. 59) terms in static or rotating samples, respectively; which in turn depend on the angle between the coil and the magnetic field, θ_C. The consequences will be discussed further below for the cases of static and rotating samples.

4.1. Static samples

Fig. 2a shows the distribution in amplitude and phase of the overtone parameter ξ in a static powder sample (Eq. 33). We have used the ^{14}N parameters of glycine and a field of B_0 = 11.74 T for comparison with the previously reported simulations and experimental results.[63,64] In this case, $|\xi|$ ranges from 0 to 1.5% and therefore both the overtone *rf* excitation and detection are much reduced. Furthermore, Fig.2a also shows that the phase of this complex parameter is randomly distributed as a result of the distributed orientations of the quadrupolar tensor with respect to the magnetic field. This random phase distribution may lead to a confusing physical picture as opposed to conventional NMR. In the latter case: (i) *rf* excitation and signal detection are usually coherent for all spins; (ii) the polarizations from all crystallites align with the magnetic field before excitation and they remain coherent after excitation; and (iii) this coherent alignment leads to an overall NMR signal with almost no cancellation. As a result, we often relate the spin polarization directly with the NMR signal. All these facts are no longer true for $^{14}N^{OT}$ NMR due to the random phase distribution of ξ. One may then wonder why it is still possible to detect $^{14}N^{OT}$ signals. Indeed, if the overtone DQ polarization was excited uniformly, in a similar way as the excitation of multiple-quantum coherences in MQMAS, then a powder average of ξ during overtone detection would annihilate the signal. The key point to overtone NMR is that the same overtone parameter ξ and its phase distribution apply for signal detection *and rf* excitation at twice the Larmor frequency. Therefore, the two phase distributions cancel each other and result in a $^{14}N^{OT}$ signal proportional to the magnitude of ξ (see Eq. 41), which is observable even for a powder sample. Nevertheless, the excitation and detection profiles depend on $|\xi|$, which makes the line shape sensitive to the excitation pulse length. In the short pulse limit, $\sin(2|\xi|\omega_1\tau_p) \approx 2|\xi|\omega_1\tau_p$, and the overtone peak intensity is proportional to the square of the overtone parameter:

$$s(\omega) \propto |\xi|^2 \tag{66}$$

Figs. 2b and 2c show that the short-pulse static line shape varies with the angle θ_C between the *rf* coil and $\boldsymbol{B}_0$, a feature unique to $^{14}N^{OT}$ NMR. Overall, only the magnitude of the overtone parameter $|\xi|$ needs be considered. For $^{14}N^{OT}$ excitation, the spin dynamics is then almost identical to that of spin $S = 1/2$ nuclei, except for the *rf* scaling and its anisotropic angular dependence. However, as a general rule, the effective overtone *rf* field is proportional to $\omega_1|\xi|$ (Eq. 37), and hence to $\omega_1\omega_Q/\omega_0$. The practical consequences of the scaled down effective *rf* field lead to (i) long pulse durations with small excitation bandwidths, (ii) difficulties in generating $^{14}N^{OT}$ spin-echoes without loss of efficiency and line shape distortions, and (iii) non-uniform excitation due to the anisotropic angular dependence.

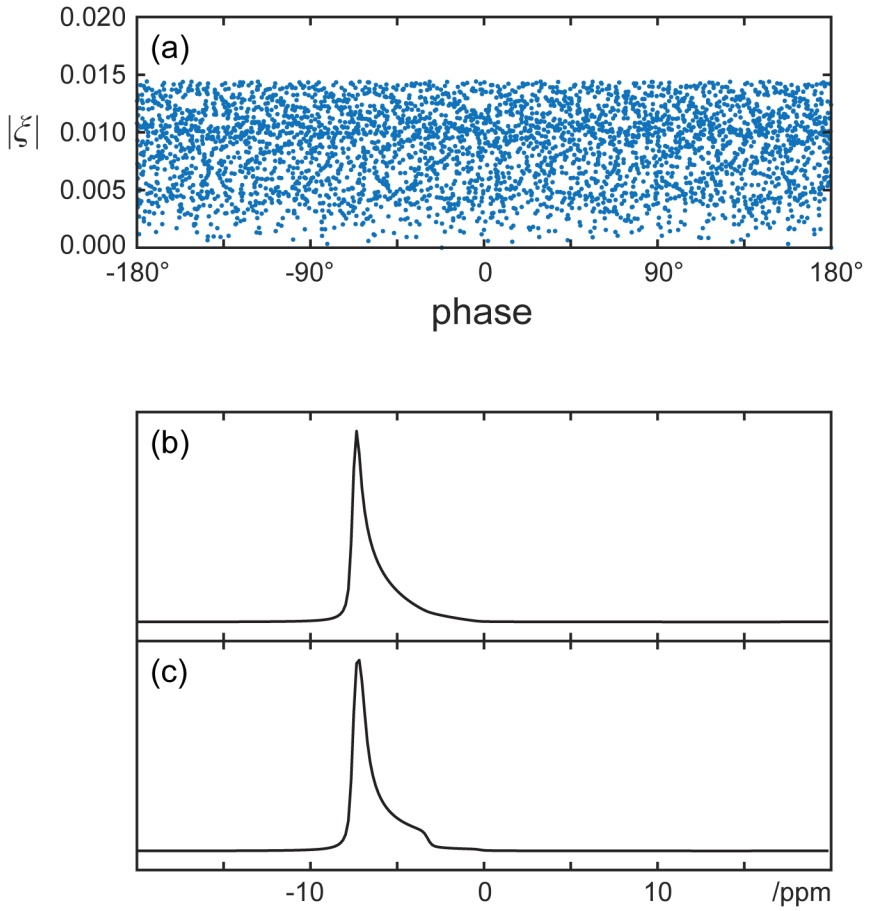

Fig. 2. Simulations of $^{14}N^{OT}$ NMR data under static conditions with B_0 = 11.74 T ($\omega_{0,14N}/(2\pi)$ = 36.118 MHz), a short pulse, and the parameters of glycine (C_Q = 1.18 MHz, η_Q = 0.53, δ_{iso} = 6 ppm). (a) Distribution of the magnitude and

phase of overtone parameter ξ, with $\theta_C = 54.74°$. Line shapes with *rf* coil (b) perpendicular or (c) parallel to the magnetic field $\boldsymbol{B}_0$. The overtone signal was scaled by $|\xi|^2$ as in Eqs. 33 and 66.

4.2. Magic-Angle Spinning samples

For rotating solids, MAS probes are usually used for $^{14}N^{OT}$ NMR to cancel the CSA and dipolar interactions, and both the spinning and coil axes are co-linear and at the magic-angle with respect to the magnetic field $\boldsymbol{B}_0$, i.e., $\theta_C = \theta_M = 54.74°$. From Eq. 62, we obtain the following numerical values for the amplitude of the five overtone components under MAS,

$$\chi_k(\theta_M) = (0.11, 0.27, 0.23, -0.25, -0.88)\ (k = 2, 1, 0, -1, -2) \qquad (67)$$

In the short pulse limit, the overtone peak intensities of the five resonances are proportional to the square of the overtone parameter:

$$ssb_k \propto |\boldsymbol{\xi}_k|^2. \qquad (68)$$

Thus, the *relative* amplitudes of the five $^{14}N^{OT}$ 'spinning sidebands' (ssbs) are given by

$$ssb_k(\theta_M) = (0.02, 0.09, 0.07, 0.09, 1.00)\ (k = 2, 1, 0, -1, -2) \qquad (69)$$

The term 'spinning sidebands' is retained as these peaks also shift with the spinning frequency. However, there are fundamental differences in the physical origin and behavior of the $^{14}N^{OT}$ ssbs as compared to spinning sidebands observed in conventional MAS experiments. For conventional NMR, the center-band is usually the dominant peak under fast spinning, whereas for overtone NMR it is the $k = -2$ sideband. The other overtone ssbs are at least an order of magnitude smaller, which makes the most prominent overtone signal appear to shift by twice the spinning frequency. Furthermore, the relative intensity of the ssbs in overtone spectra are mostly independent of spinning frequency.

It should be noted that if the spinning axis is inverted with respect to $\boldsymbol{B}_0$, i.e., $\theta_M \rightarrow 180° - \theta_M$ or equivalently $\omega_r \rightarrow -\omega_r$, the relative amplitudes of the overtone ssbs, which are proportional to $|\xi_k|^2$ in the short pulse regime (Eq.66), reverse in order (Eq. 62),

$$ssb_k(\pi - \theta_M) = (1.00, 0.09, 0.07, 0.09, 0.02)\ (k = 2, 1, 0, -1, -2) \qquad (70)$$

The $k = 2$ sideband becomes dominant and the main signal shifts by twice the spinning frequency in the opposite direction. $^{14}N^{OT}$ NMR is a rare case where the spectra are sensitive to the sense of spinning with respect to the magnetic field.

Fig. 3 shows simulations of the $^{14}N^{OT}$ NMR line shape and relative sideband intensities in the short pulse regime (see Eq. 70) versus the spinning/coil axis angle θ_C. As stated previously, the order of the sidebands is reversed ($k \leftrightarrow -k$) for θ_C and $180° - \theta_C$, as observed when $\theta_C = 54.7°$ and 125.3°, while the line shape remains the same for the individual sidebands. When the axis is parallel (or anti-parallel) to $\boldsymbol{B}_0$, only the sideband at $-2\omega_r$ (or $+2\omega_r$) exists. As θ_C increases up to the magic-angle, the $k = -2$ $^{14}N^{OT}$ sideband remains dominant. The other sidebands increase rapidly in intensity as θ_C approaches 90°. When the rotor axis is perpendicular to $\boldsymbol{B}_0$ ($\theta_C = 90°$), the sideband intensities are symmetric as expected from symmetry considerations and reversing the spinning direction does not affect the spectrum.

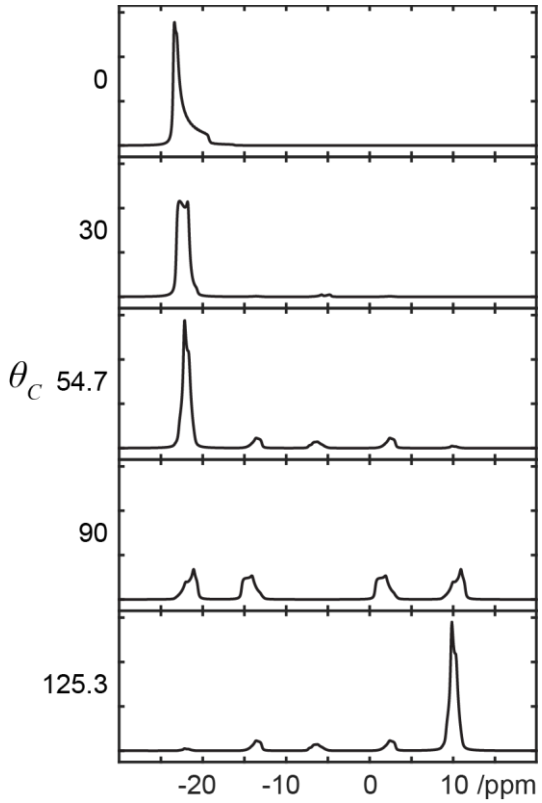

Fig. 3. Simulations of $^{14}N^{OT}$ short-pulse spectra under rotation at various θ_C angles of the spinning/coil axis, with $\boldsymbol{B}_0$ = 11.74 T, $\omega_{0,14N}/(2\pi)$ = 36.118 MHz, $\omega_R/(2\pi)$ = 8 kHz, and the parameters of glycine (see Fig. 2 caption). The overtone peaks were scaled by $|\xi_k|^2$.

The time modulation of the overtone excitation and detection can be expressed by combining Eqs. 58 and 60 and it introduces two intriguing questions.

$$\xi_{rot}(t,\theta_M) = \varepsilon \sum_{k=-2}^{2} \chi_k(\theta_M) \sum_{m=-2}^{2} A_{2,m}^{Q,P} d_{m,k}^{2}(\beta_{PR}) \times \exp(-i[m\alpha_{PR} + k(\omega_r t + \gamma_{PR})]) \quad (71)$$

First, the most prominent overtone peak shifts at twice the spinning frequency, while its energy level remains at the center band position, i.e., at the time averaged frequency over one rotor period. By placing the *rf* carrier frequency onto the main overtone peak position, i.e., at the $-2\omega_r$ sideband, is the *rf* irradiation on- or off-resonance? The answer is that the *effective* excitation is on-resonance. Although the *rf* irradiation is offset by $2\omega_r$, the modulation of the *rf* field by the $2\omega_r$ component in Eq. 71 effectively makes the overtone irradiation frequency match the overtone DQ transition. Second, the five modulating *k* components of Eq. 71 can all excite the overtone transition despite

their frequency offsets. How much does each of the five modulating k components mutually contribute to other overtone ssbs? In other words, can the dominant modulating component be used to excite the other smaller overtone sidebands? The answer to the second question is that only excitation from the same modulating component contributes to the sideband being observed. The reason lies in the effect of the rotor angle γ_{PR} on the overtone *rf* field, which appears in Eq. 71 as the phase $k\gamma_{PR}$. In the linear excitation regime, the excitations from other components have a non-vanishing γ_{PR} angular dependence given by $\exp(i[k_{exc} - k_{det}]\gamma_{PR})$, which is annihilated by powder averaging; k_{exc} and k_{det} are the modulating sideband orders for the excitation and detection, respectively. Thus, only the excitation from the same sideband component (i.e., $k_{exc} = k_{det}$) contributes to the overtone peak being observed. In the short pulse limit, the peak intensities of the overtone sidebands are given by the square of the relative amplitude ξ_k which effectively amplifies the differences in relative intensity and makes the $\pm 2\omega_r$ peak appearing more dominant under MAS.

Fig. 4 shows experimental $^{14}N^{OT}$ MAS spectra of glycine at ν_r = 10 kHz, with the *rf* carrier frequency set on each of the five observed sidebands. The $^{14}N^{OT}$ peak intensities agree with the simulated results for the relative sideband intensities in Fig.3. In order to confirm the dependence of the spinning induced $^{14}N^{OT}$ MAS shift on the sense of spinning relative to the magnetic field, we have searched all possible magnet and probe combinations available to us and found that all vertical-bore superconducting NMR magnets we have access to have their magnetic fields pointing upwards. Most of the MAS probes are equipped with spinning modules from Bruker and Revolution NMR which (coincidentally?) spin samples in the same direction (counterclockwise when looking down the coil/stator axis). Only one of our decommissioned Doty probes spins the samples in the opposite direction which allowed us to confirm experimentally that the spinning

induced shift of the main overtone peak is reversed in the 'opposite' spinning direction. Agreement has also been observed from $^{14}N^{OT}$ MAS NMR spectra acquired later using JEOL probes which also spin in the clockwise direction (not shown). Experimentally, long *rf* pulses are usually used in order to observe sufficient signal intensity. The narrow excitation bandwidth of long pulses makes the simultaneous observation of all five sidebands difficult. The five sidebands in Fig. 4 were acquired individually by placing the overtone *rf* frequency on each of the marked peak positions in Fig. 4.

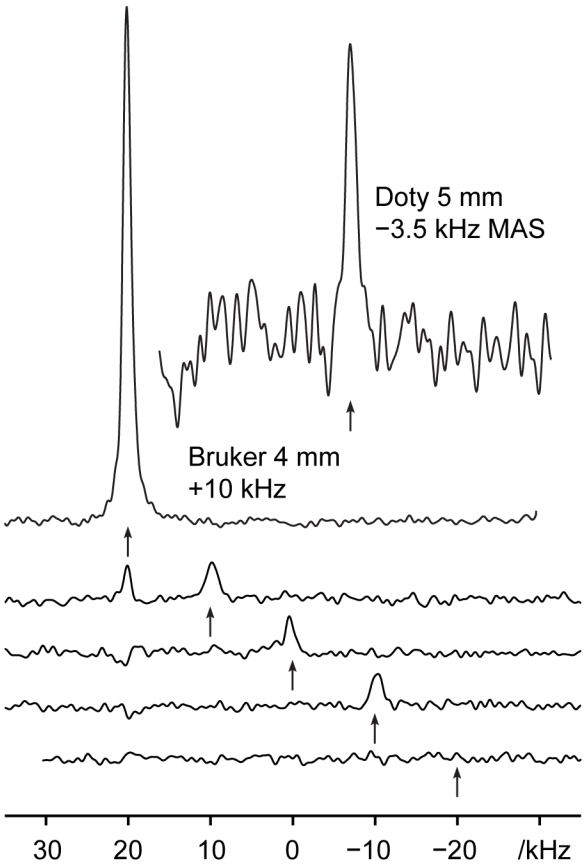

Fig. 4. Experimental $^{14}N^{OT}$ MAS spectra of glycine recorded at 19.6 T, with $\omega_R/(2\pi)$ = 10 and 3.5 kHz using a 4 mm Bruker and 5 mm Doty MAS probes with approximately 70 and 110 μl sample volume, respectively. The *rf* amplitude $\omega_1/(2\pi)$ was calibrated using a D_2O sample and was approximately 60 and 20 kHz for the Bruker and Doty probe, respectively. The deuterium Larmor frequency is within 6% of the ^{14}N overtone frequency. 100 and 50 μs long excitation pulses were used for the Bruker and Doty probes with frequency offsets set on resonance with respect to the overtone peaks indicated by the arrows. The recycle delay was 0.5 s and the number of scans were 1024 for measuring the main -2 sideband, 32768 for the other sidebands of the Bruker 4 mm experiment and 102400 for the Doty 5 mm experiment. The two probes spin the samples in opposite directions/senses with respect to $\boldsymbol{B}_0$. The spectra recorded with the Bruker probe were acquired using five different carrier frequencies denoted by the arrows. Only one spectrum with the frequency set at the expected main overtone peak position was acquired using the Doty probe due to the weak signal caused by the low *rf* field. The results confirm the second spinning sideband as the main overtone

peak, which is shifted by twice the spinning frequency in a direction determined by the spinning axis relative to the magnetic field.

The National High Magnetic Field Laboratory has recently commissioned a 36 Tesla series-connected-hybrid magnet with field homogeneity and stability suitable for high-resolution solid-state NMR experiments.[10] The powered magnet can be ramped to the full field strength in either direction in approximately 30 minutes. Thus, $^{14}N^{OT}$ MAS NMR spectra can be acquired back-to-back spinning in the same direction but with opposite field orientations in about an hour. Fig. 5 shows the $^{14}N^{OT}$ MAS NMR spectra of glycine with the magnetic field in opposite directions. In addition, $^{14}N^{OT}$ MAS spectra were acquired at two spinning frequencies to show the spinning induced shift of the $2\omega_r$ overtone sideband. The lower peak intensities at $\omega_R/2\pi = 5$ kHz are due to the fact that the single-channel probe used relies solely on MAS to average the dipolar coupling to the protons. Low spinning causes less efficient decoupling, contributing to broader overtone lines and lower intensities. The results confirm again the opposite spinning induced shift of ^{14}N overtone peaks with respect to the magnetic field direction.

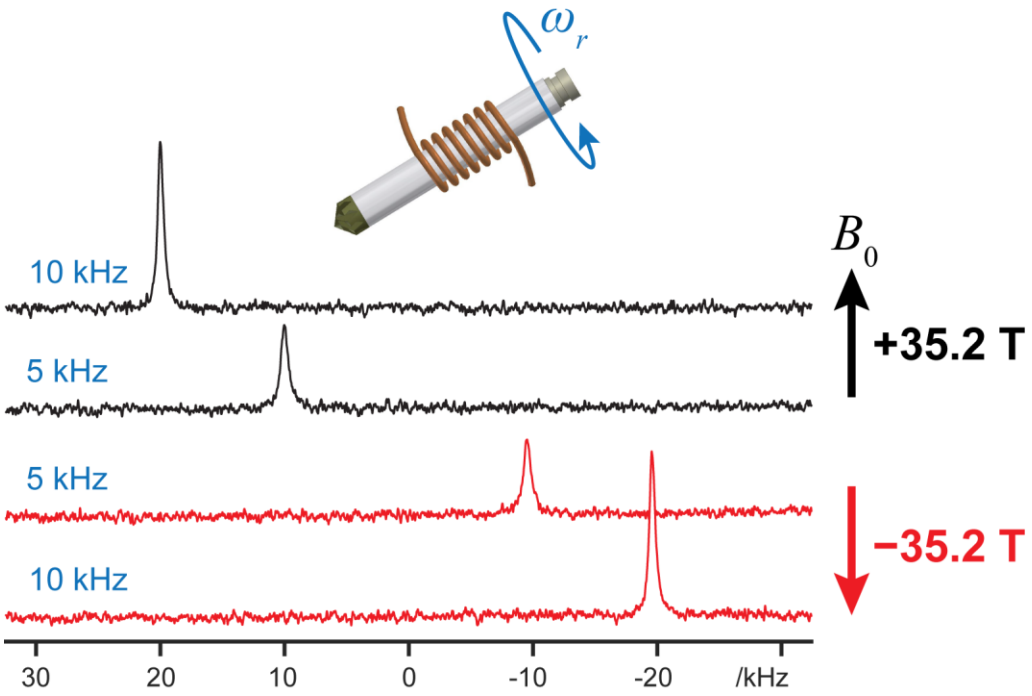

Fig. 5. Experimental $^{14}N^{OT}$ MAS NMR spectra of glycine recorded at 35.2 T using the series-connected-hybrid (SCH) magnet at the National High Magnetic Field Laboratory. A 3.2 mm home-built MAS probe with 36 μl sample volume was used for the measurement. A 400 μs pulse with approximately 100 kHz *rf* field was used for the overtone excitation. The frequency offset was placed at the main overtone peaks. 8192 scans with 0.1 s recycle delay were acquired for each spectrum. Two sets of spectra were acquired back-to-back by reversing the direction of the magnetic field for $\omega_R/(2\pi)$ = 5 and 10 kHz spinning frequencies.

5. Conclusions

We have shown than overtone NMR of ^{14}N nuclei, or more generally of any spin S = 1 nucleus, can be described by an overtone parameter in the case of static or rotating samples. This parameter, which scales down both the effective *rf* field and the detected signal, depends on the quadrupolar coupling interaction and the crystallite orientation, and is inversely proportional to the magnetic field. The spin dynamics of overtone excitation can be treated as a fictitious spin S = 1/2 nucleus represented by a two-level overtone transition and a *rf* field scaled down by the overtone parameter. For rotating samples, the overtone parameter is modulated by the spinning, which gives rise to five components or spinning sidebands. The relative amplitudes of the five sidebands are only determined by the orientation of the *rf* coil and the spinning axis with respect to the magnetic field. For a solenoid coil and spinning axis along the magic angle, the relative signal amplitudes are (0.02, 0.09, 0.07, 0.09, 1.00). Thus, the $2\omega_r$ sideband dominates and the main observable overtone peak appears shifted, at twice the spinning frequency. Reversing the spinning (or magnetic field) direction makes the peak shift in the opposite direction. The presented theory gives a physical explanation for the intriguing features observed in the overtone NMR spectra of rotating samples, and a simple formalism for the spin dynamics therein. The understanding and presented formalism will help in exploiting $^{14}N^{OT}$ NMR for the highly abundant nitrogen isotope.

Acknowledgements

This work was supported by the National High Magnetic Field Laboratory through National Science Foundation Cooperative Agreement (DMR-1644779) and by the State of Florida. Development of the SCH magnet and NMR instrumentation was supported by NSF (DMR-1039938 and DMR-0603042). JT, OL and JPA also acknowledge contract CEFIPRA n°85208-E, PRC CNRS-NSFC and ANR-17-ERC2-0022 (EOS). HN acknowledges the Univ. Lille and Région Hauts-de-France for his PhD grant. BH acknowledges National Natural Science Foundation of China for Excellent Young Scholars (Grant No. 21522303). YN acknowledges JSPS KAKENHI (Grant number JP17H03043).

References

[1] E. R. Andrew, A. Bradbury, and R. G. Eades, Nature (London, U. K.) **183**, 1802 (1959).
[2] J. Schaefer and E. O. Stejskal, J. Am. Chem. Soc. **98** (4), 1031 (1976).
[3] A. Samoson, E. Lippmaa, and A. Pines, Mol. Phys. **65** (4), 1013 (1988).
[4] A. Llor and J. Virlet, Chem. Phys. Lett. **152** (2-3), 248 (1988).
[5] K. T. Mueller, B. Q. Sun, G. C. Chingas, J. W. Zwanziger, T. Terao, and A. Pines, J. Magn. Reson. **86** (3), 470 (1990).
[6] L. Frydman and J. S. Harwood, J. Am. Chem. Soc. **117** (19), 5367 (1995).
[7] Z. H. Gan, J. Am. Chem. Soc. **122** (13), 3242 (2000).
[8] Z. Gan, H. T. Kwak, M. Bird, T. Cross, P. Gor'kov, W. Brey, and K. Shetty, J. Magn. Reson. **191** (1), 135 (2008).
[9] Z. H. Gan, P. Gor'kov, T. A. Cross, A. Samoson, and D. Massiot, J. Am. Chem. Soc. **124** (20), 5634 (2002).
[10] Z. H. Gan, I. Hung, X. L. Wang, J. Paulino, G. Wu, I. M. Litvak, P. L. Gor'kov, W. W. Brey, P. Lendi, J. L. Schiano, M. D. Bird, L. R. Dixon, J. Toth, G. S. Boebinger, and T. A. Cross, J. Magn. Reson. **284**, 125 (2017).
[11] M. E. Smith and E. R. H. van Eck, Prog. Nucl. Magn. Reson. Spectrosc. **34** (2), 159 (1999).
[12] P. M. J. Szell and D. L. Bryce, in *Annual Reports on NMR Spectroscopy, Vol 84* (2015), Vol. 84, pp. 115.
[13] P. Pyykko, Mol. Phys. **116** (10), 1328 (2018).
[14] K. J. D. Mackenzie, R. H. Meinhold, D. G. McGavin, J. A. Ripmeester, and I. Moudrakovski, Solid State Nucl. Magn. Reson. **4** (4), 193 (1995).
[15] T. J. Bastow, D. Massiot, and J. P. Coutures, Solid State Nucl. Magn. Reson. **10** (4), 241 (1998).
[16] G. Jeschke and M. Jansen, Angew. Chem.-Int. Edit. **37** (9), 1282 (1998).
[17] A. K. Khitrin and B. M. Fung, J. Chem. Phys. **111** (19), 8963 (1999).

[18] E. Konstantin and B. M. Fung, J. Chem. Phys. **110** (16), 7977 (1999).
[19] M. Fechtelkord, A. Engelhardt, J. C. Buhl, L. Schwalowsky, and U. Bismayer, Solid State Nucl. Magn. Reson. **17** (1-4), 76 (2000).
[20] H. J. Jakobsen, H. Bildsoe, J. Skibsted, and T. Giavani, J. Am. Chem. Soc. **123** (21), 5098 (2001).
[21] T. Giavani, H. Bildsoe, J. Skibsted, and H. J. Jakobsen, J. Phys. Chem. B **106** (11), 3026 (2002).
[22] T. Giavani, H. Bildsoe, J. Skibsted, and H. J. Jakobsen, Chem. Phys. Lett. **377** (3-4), 426 (2003).
[23] T. Giavani, H. Bildsoe, J. Skibsted, and H. J. Jakobsen, J. Magn. Reson. **166** (2), 262 (2004).
[24] B. Zhou, T. Giavani, H. Bildsoe, J. Skibsted, and H. J. Jakobsen, Chem. Phys. Lett. **402** (1-3), 133 (2005).
[25] A. R. Hove, H. Bildsoe, J. Skibsted, M. Brorson, and H. J. Jakobsen, Inorg. Chem. **45** (26), 10873 (2006).
[26] H. J. Jakobsen, A. R. Hove, R. G. Hazell, H. Bildsoe, and J. Skibsted, Magn. Reson. Chem. **44** (3), 348 (2006).
[27] H. J. Jakobsen, H. Bildsoe, J. Skibsted, M. R. Hansen, M. Brorson, B. R. Srinivasan, and W. Bensch, Inorg. Chem. **48** (5), 1787 (2009).
[28] L. A. O'Dell and R. W. Schurko, J. Am. Chem. Soc. **131** (19), 6658 (2009).
[29] L. A. O'Dell and R. W. Schurko, Phys. Chem. Chem. Phys. **11** (32), 7069 (2009).
[30] B. E. G. Lucier, A. R. Reidel, and R. W. Schurko, Canadian Journal of Chemistry-Revue Canadienne De Chimie **89** (7), 919 (2011).
[31] T. Mineva, P. Gaveau, A. Galarneau, D. Massiot, and B. Alonso, Journal of Physical Chemistry C **115** (39), 19293 (2011).
[32] L. A. O'Dell, R. W. Schurko, K. J. Harris, J. Autschbach, and C. I. Ratcliffe, J. Am. Chem. Soc. **133** (3), 527 (2011).
[33] L. A. O'Dell, Prog. Nucl. Magn. Reson. Spectrosc. **59** (4), 295 (2011).
[34] E. Dib, T. Mineva, P. Gaveau, and B. Alonso, Phys. Chem. Chem. Phys. **15** (42), 18349 (2013).
[35] B. E. G. Lucier, K. E. Johnston, W. Q. Xu, J. C. Hanson, S. D. Senanayake, S. Y. Yao, M. W. Bourassa, M. Srebro, J. Autschbach, and R. W. Schurko, J. Am. Chem. Soc. **136** (4), 1333 (2014).
[36] S. L. Veinberg, Z. W. Friedl, K. J. Harris, L. A. O'Dell, and R. W. Schurko, Crystengcomm **17** (28), 5225 (2015).
[37] S. L. Veinberg, Z. W. Friedl, A. W. Lindquist, B. Kispal, K. J. Harris, L. A. O'Dell, and R. W. Schurko, ChemPhysChem **17** (23), 4011 (2016).
[38] S. L. Veinberg, K. E. Johnston, M. J. Jaroszewicz, B. M. Kispal, C. R. Mireault, T. Kobayashi, M. Pruski, and R. W. Schurko, Phys. Chem. Chem. Phys. **18** (26), 17713 (2016).
[39] M. Shen, Q. Chen, J. P. Amoureux, and B. W. Hu, Solid State Nucl. Magn. Reson. **78**, 5 (2016).
[40] G. N. M. Reddy, M. Malon, A. Marsh, Y. Nishiyama, and S. P. Brown, Analytical Chemistry **88** (23), 11412 (2016).
[41] M. K. Pandey, J. P. Amoureux, T. Asakura, and Y. Nishiyama, Phys. Chem. Chem. Phys. **18** (32), 22583 (2016).
[42] M. Shen, J. Trebosc, L. A. O'Dell, O. Lafon, F. Pourpoint, B. W. Hu, Q. Chen, and J. P. Amoureux, J. Magn. Reson. **258**, 86 (2015).

[43] L. A. O'Dell, R. L. He, and J. Pandohee, Crystengcomm **15** (43), 8657 (2013).
[44] Y. Nishiyama, M. Malon, Z. H. Gan, Y. Endo, and T. Nemoto, J. Magn. Reson. **230**, 160 (2013).
[45] J. Fukazawa, S. Kato, T. Ozaki, A. Shoji, and K. Takegoshi, J. Am. Chem. Soc. **132** (12), 4290 (2010).
[46] R. Siegel, J. Trebosc, J. P. Amoureux, and Z. Gan, J. Magn. Reson. **193** (2), 321 (2008).
[47] Z. H. Gan, Chem. Commun. (7), 868 (2008).
[48] S. Antonijevic and N. Halpern-Manners, Solid State Nucl. Magn. Reson. **33** (4), 82 (2008).
[49] S. Cavadini, S. Antonijevic, A. Lupulescu, and G. Bodenhausen, ChemPhysChem **8** (9), 1363 (2007).
[50] Z. H. Gan, J. P. Amoureux, and J. Trebosc, Chem. Phys. Lett. **435** (1-3), 163 (2007).
[51] Z. H. Gan, J. Magn. Reson. **184** (1), 39 (2007).
[52] Z. H. Gan, J. Am. Chem. Soc. **128** (18), 6040 (2006).
[53] S. Cavadini, S. Antonijevic, A. Lupulescu, and G. Bodenhausen, J. Magn. Reson. **182** (1), 168 (2006).
[54] K. Takegoshi, T. Yano, K. Takeda, and T. Terao, J. Am. Chem. Soc. **123** (43), 10786 (2001).
[55] M. Bloom, private communication.
[56] M. Legros, M.Sc., University of British Columbia, 1984.
[57] R. Tycko and S. J. Opella, J. Chem. Phys. **86** (4), 1761 (1987).
[58] D. K. Lee and A. Ramamoorthy, Chem. Phys. Lett. **286** (5-6), 398 (1998).
[59] D. K. Lee and A. Ramamoorthy, Chem. Phys. Lett. **286** (5-6), 403 (1998).
[60] D. K. Lee and A. Ramamoorthy, Chem. Phys. Lett. **280** (5-6), 501 (1997).
[61] L. Marinelli, S. Wi, and L. Frydman, J. Chem. Phys. **110** (6), 3100 (1999).
[62] N. M. Trease and P. J. Grandinetti, J. Chem. Phys. **128** (5) (2008).
[63] L. A. O'Dell and C. I. Ratcliffe, Chem. Phys. Lett. **514** (1-3), 168 (2011).
[64] L. A. O'Dell and A. Brinkmann, J. Chem. Phys. **138** (6) (2013).
[65] I. M. Haies, J. A. Jarvis, L. J. Brown, I. Kuprov, P. T. F. Williamson, and M. Carravetta, Phys. Chem. Chem. Phys. **17** (37), 23748 (2015).
[66] R. R. Ernst, G. Bodenhausen, and A. Wokaun, *Principles of Nuclear Magnetic Resonance in One and Two Dimensions*. (Oxford University Press, New York, 1987).
[67] S. Cavadini, A. Lupulescu, S. Antonijevic, and G. Bodenhausen, J. Am. Chem. Soc. **128** (24), 7706 (2006).
[68] A. J. Pell, K. J. Sanders, S. Wegner, G. Pintacuda, and C. P. Grey, J. Chem. Phys. **146** (19) (2017).
[69] N. T. Duang, I. Kuprov, and Y. Nishiyama, presented at the 10th Alpine Conference on Solid-State NMR, Chamonix Mont-Blanc, France, 2017 (unpublished).
[70] N. T. Duong, I. Kuprov, and Y. Nishiyama, J. Magn. Reson. **291**, 27 (2018).
[71] M. Goldman, P. J. Grandinetti, A. Llor, Z. Olejniczak, J. R. Sachleben, and J. W. Zwanziger, J. Chem. Phys. **97** (12), 8947 (1992).
[72] C. L. Mayne, *Liouville equation of motion*. (John Wiley & Sons Ltd., Chichester, UK, 2012).
[73] J. H. Shirley, Phys. Rev. **138** (4B), B979 (1965).
[74] M. Leskes, P. K. Madhu, and S. Vega, Prog. Nucl. Magn. Reson. Spectrosc. **57** (4), 345 (2010).
[75] M. V. Berry, Proceedings of the Royal Society of London Series a-Mathematical and Physical Sciences **392** (1802), 45 (1984).
[76] R. Tycko, Phys. Rev. Lett. **58** (22), 2281 (1987).

[77] A. Brinkmann and L. A. O'Dell, Solid State Nucl. Magn. Reson. **84**, 34 (2017).